ON THE BENEFICIAL EFFECT OF MgO PROMOTER ON THE PERFORMANCE OF CO_3O_4/Al_2O_3 CATALYSTS FOR COMBUSTION OF DILUTE METHANE

A. Choya, B. de Rivas, J.R. González-Velasco, J.I. Gutiérrez-Ortiz, R. López-Fonseca

Applied Catalysis A: General 582 (2019) 117099

DOI: 10.1016/j.apcata.2019.05.033

ON THE BENEFICIAL EFFECT OF MgO PROMOTER ON THE PERFORMANCE OF Co_3O_4/Al_2O_3 CATALYSTS FOR COMBUSTION OF DILUTE METHANE

Andoni Choya, Beatriz de Rivas, Juan Ramón González-Velasco

Jose Ignacio Gutiérrez-Ortiz, Rubén López-Fonseca*

Chemical Technologies for Environmental Sustainability Group,

Department of Chemical Engineering, Faculty of Science and Technology,

University of The Basque Country UPV/EHU, PO Box 644, E-48080 Bilbao, Spain

*Corresponding author:

Phone: +34-94-6015985

Fax: +34-94-6015963

E-mail address: ruben.lopez@ehu.eus

ABSTRACT

The present work deals with the analysis of a series of cobalt catalysts (20 and 30%wt.Co) supported on alumina modified with MgO (7-18%wt.Mg with respect to the support) for the combustion of dilute methane. Both modified supports and the resulting cobalt catalysts were characterised by N_2 physisorption, wavelength dispersive X-ray fluorescence, X-ray diffraction, Raman spectroscopy and temperature-programmed reduction with hydrogen. A beneficial effect on catalytic activity was found with respect to the reference samples supported on blank alumina. As evidenced by the kinetic results in terms of specific reaction rate and apparent activation energy, this positive influence was related to a partial inhibition generation of less active $CoAl_2O_4$ due to MgO coverage of the support in favour of increasing the amount of easily reducible cobalt species, mainly in the form of Co_3O_4. The optimum magnesium loading was 12%wt. irrespective of the cobalt content, while the catalysts with 30%wt.Co were significantly more active than their counterparts with 20%wt.Co. Finally, a good catalytic stability with time on stream (150 hours) was observed.

Keywords: methane oxidation, cobalt oxide, alumina supported catalysts, magnesium oxide

1. Introduction

Methane is a powerful greenhouse effect gas with a global warming potential of around 28 for a 100-year period, and it accounts for around 20% of the total radiative forcing from all greenhouse gases [1,2] From all the anthropogenic sources, energy production and transport seem to be the two sectors that produce the most emissions of methane. Facilities such as oil refineries or natural gas plants and natural gas engines usually release low concentrations of methane that are difficult to remove due to the high stability of this molecule [3,4]. Since these off-gases are generally characterised by large flows at low to moderate temperatures, catalytic oxidation is the preferred abatement technique. Traditionally, catalysts for this application are based on noble metals such as palladium and platinum. However, nowadays there is an increasing interest on substituting these materials by cheaper systems, namely transition metal oxides with a defined structure such as spinels, perovskites or hexaaluminates, which can be equally active and stable [5-7].

Spinel oxides, and in particular, spinel-type cobalt oxide (Co_3O_4) is a widely known material that can serve as an alternative to noble metals for catalytic oxidation due to its good redox properties [8-11]. However, its generally poor structural and textural properties tend to hinder the potential activity of this material, especially when it is prepared by conventional synthesis methodologies [10,11]. One possible solution to this problem could be to support the cobalt oxide over the surface of a porous media, in order to increase the amount of surface area available for the reaction. Although this option generally enhances the structural properties of the catalyst, it also presents a major drawback related to the fact that the cobalt-support interaction almost invariably has a detrimental effect on the redox properties of supported Co_3O_4, thus balancing out the benefits of improved structural properties [12,13]. Specifically when the chosen support

is alumina, the cobalt-support interaction also leads to the formation of an inactive cobalt aluminate phase ($CoAl_2O_4$) characterised by a poor reducibility [14,15]. A proposed solution already found in the bibliography has been the modification of the support with the purpose of altering its stability and affinity for the cobalt oxide supported over it. This can be addressed by adding some chemical promoters to the alumina support before the incorporation of Co_3O_4, or by adding these promoters to the final Co/Al_2O_3 catalyst. In this sense, Cheng at al. [16] found that Cu-Co mixed oxide catalysts supported over modified alumina obtained by a co-precipitation method were highly active for methane oxidation, especially when the alumina was modified with manganese. On the other hand, El-Shobaky et al. [17] reported an increased activity of Co_3O_4/Al_2O_3 catalysts for CO oxidation when these were doped with small amounts of manganese and/or lanthanum. Alternatively, using magnesium as a modifier for this type of catalysts seems to be a good way to improve their performance. For instance, Riad [18] found that magnesium-modified alumina prepared by co-precipitation exhibited better textural and structural properties than bare alumina. Magnesium oxide can be also used as a support for cobalt catalysts as well, thereby resulting in systems with an improved activity owing to the magnesium-cobalt interaction as reported by Ulla et al. [12] and Ji et al. [19]

In this context, the present investigation is based on our previous results on the comparison of bulk and supported Co_3O_4 catalysts, and more particularly, on the effect of Co loading (10-40%wt.Co) for the combustion of methane on Co_3O_4/Al_2O_3 catalysts [20,21]. Thus, the best results were found for the 20-30%wt. loadings. This work aims at designing improved supported catalysts by means of surface protection of the alumina support before incorporation of the Co_3O_4 phase. To the best of our knowledge, there are no research studies in the available literature regarding the use of this type of catalysts for this environmental application. On the basis of the fact that the deposited MgO should act

as a physical barrier between deposited cobalt and the alumina support, thereby limiting the cobalt-alumina interaction and the subsequent cobalt aluminate formation, the objective will be to study the catalytic behaviour of a set of cobalt catalysts with varying metallic loading (20 and 30%wt.) supported on three different modified-alumina supports (7-18%wt.Mg) for the oxidation of trace amounts of methane.

2. Experimental

2.1. Catalysts preparation

The magnesium-modified alumina supports were prepared by precipitation of a magnesium precursor on a commercial γ-alumina (Saint-Gobain), which was previously thermally stabilised at 850 ºC for 4 hours in static air. For each support, 5 g of γ-alumina were mixed with 100 mL of magnesium (II) nitrate hexahydrate ($Mg(NO_3)_2 \cdot 6H_2O$, Merck) with adjusted concentrations of Mg. Then, a solution of Na_2CO_3 1.2M was added drop-by-drop while the temperature of the mixture was kept at 80 °C, until the pH was 8.5. The selected magnesium loadings were 7, 12 and 18%wt.Mg. The obtained precipitates were collected and washed with at least 5 litres of water to eliminate all the residual sodium ions from the precursor. These supports were denoted as x$Mg\text{-}Al_2O_3$ where x stands for the measured magnesium loading. On the other hand, a support of pure magnesia (MgO) was also prepared by applying the same precipitation route using a magnesium nitrate solution.

Supported $Co/Mg\text{-}Al_2O_3$, Co/Al_2O_3 and Co/MgO catalysts were prepared following the same precipitation route as the supports but starting with a mixture of 5 g of each support in powder form and 100 mL of cobalt (II) nitrate hexahydrate ($Co(NO_3)_2 \cdot 6H_2O$, Alfa Aesar) with adjusted concentrations of Co. The chosen Co loadings were 20 and 30%wt. These samples were denoted as y$Co/xMg\text{-}Al_2O_3$ where y stands for the cobalt loading.

All supports and catalyst precursors were dried in static air at 110 °C for 16 hours and then subjected to calcination in static air to produce the final supports and catalysts. The calcination protocol involved three heating ramps separated with two 30-minute isotherms: an initial ramp from ambient temperature up to 125 °C at 5 °C min^{-1}, an intermediate ramp from 125 to 300 °C at 1 °C min^{-1} and a final ramp at 5 °C min^{-1} up to 600 °C, which was the maintained for 4 hours. In this way, the x$Mg\text{-}Al_2O_3$ supports were calcined at 600 ºC for 4 hours in order to obtain the MgO phase. Then, the Co catalysts were submitted to an additional activation thermal step at 600 ºC for 4 hours in static air so as to induce the formation of Co_3O_4. Exceptionally, one of the Mg-modified alumina supports (18$Mg\text{-}Al_2O_3$) was also calcined at 850 °C for 4 hours. The selection of this specific thermal programme was made on the basis of the thermagravimetric analysis of the oxidative decomposition of the precipitated cobalt precursor, namely cobalt hydroxide carbonate, into Co_3O_4. Hence, it was observed that this transformation occurred in the 125-300 °C temperature range (Figure S1, Supplementary material).

A number of reference samples were also prepared since they could be useful for the interpretation of the characterisation results of the various $Mg\text{-}Al_2O_3$ supports and the examined $Co/Mg\text{-}Al_2O_3$ catalysts. These materials were bulk Co_3O_4, $CoAl_2O_4$ and $MgAl_2O_4$. Bulk Co_3O_4 was prepared following the same precipitation route detailed above, starting from a solution of cobalt nitrate (II) hexahydrate. On the other hand, bulk $CoAl_2O_4$ and $MgAl_2O_4$ were prepared by co-precipitation routes via layered double hydroxide precursors [22,23].

2.2. Characterisation techniques

Textural properties of the samples were determined from the N_2 adsorption/desorption isotherms at -196 °C obtained with a Micromeritics TriStar II apparatus. The specific

surface of the samples was obtained by the BET method, and the average pore size was calculated using the BJH method. All samples were degassed prior to analysis on a Micromeritics SmartPrep apparatus at 300 ºC for 10 hours with a N_2 flow.

The composition of the supports and catalysts was determined by Wavelength Dispersive X-Ray Fluorescence (WDXRF). From each sample in powder form, a boron glass pearl was prepared by fusion in an induction micro-furnace, by mixing the sample with the flux agent Spectromelt A12 (Merck) in an approximate proportion of 20:1. Chemical analysis of each pearl was performed under vacuum, using a PANalytical AXIOS sequential WDXRF spectrometer, equipped with a Rh tube and three different detectors (gas flow, scintillation and Xe sealed).

Structural properties of the catalysts were determined by X-Ray diffraction. XRD analysis were performed on a X'PERT-PRO X-Ray diffractometer using Cu Kα radiation (λ = 1.5406 Å) and a Ni filter. The X-Ray tube was operated at 40 kV and 40 mA of current. The samples were scanned from an initial value of 2θ = 5° to a final value of 2θ = 80°, with a step size of 0.026° and a counting time of 2.0 seconds. Phase identification was performed by comparison of the obtained diffraction patterns with JCPDS (Joint Committee on Powder Diffraction Standards) database cards.

The analysis by Raman spectroscopy was carried out by using a Renishaw InVia Raman spectrometer, coupled to a Leica DMLM microscope. The excitation wavelength was 514 nm (ion-argon laser, Modu-Laser). The spatial resolution was 2 microns. For each spectrum, 20 seconds were employed and five scans were accumulated with the 10% of the maximum power of the 514 nm laser in a spectral window of 150-1500 cm^{-1}.

Finally, temperature-programmed reduction with hydrogen (H_2-TPR) was performed on a Micromeritics Autochem 2920 apparatus, using a 5%H_2/Ar mixture as the reducing gas. The analysis protocol involved an initial pre-treatment step with a 5%O_2/He mixture at

300 °C for 30 minutes. After cooling down to room temperature with flowing He, the TPR experiment was performed, up to 950 °C for all the samples. This final temperature was then maintained for 30 minutes. The water produced throughout the whole experiment was eliminated using a cold trap, to avoid interference with the TCD detector.

2.3. Catalytic activity determination

Catalytic activity tests were performed at atmospheric pressure in a bench-scale fixed bed reactor (PID Eng&Tech S.L.) in the 300-600 C temperature range. Each reaction experiment was made by using 1 g of catalyst (particle size of 0.25-0.3 mm) diluted with the same mass of inert quartz (particle size 0.5-0.8 mm) to enhance heat and reactants distribution along the catalytic bed. The calcined samples were not submitted to any further activation treatment prior to the catalytic runs. The feedstream (1%CH_4, 10%O_2 and N_2 as the balance gas) was fed to the reactor with a total flow of 500 cm^3 min^{-1}, which corresponded to a space velocity of 300 mL CH_4 g^{-1} h^{-1} (60,000 h^{-1} approximately for an estimated catalyst density of 2 g cm^{-3}). Conversion measurements and product profiles were taken at steady state each 25 °C, typically after 15 minutes on stream. The furnace temperature was programmed in a stepwise progression. Each temperature level was attained using a heating ramp of 1 °C min^{-1}. Each chromatographic analysis was performed in triplicate in order to check reproducibility, and it was found that the standard deviation for every set of three values was always below 1%. Additionally, stability tests were carried out for a total time on stream of 150 hours at 500 ºC. Further details on the experimental set-up and the analysis of the product stream are detailed elsewhere [20]. The absence of diffusional limitations that could affect the obtained catalytic results was checked in agreement to the Eurokin procedure (see Table S1, Supplementary material). Hence, according to the obtained results for intragranular and extra-granular mass

diffusion, energy diffusion and temperature gradients, it was considered that the catalytic activity results were not significantly influenced by interphase transportation phenomena.

3. Results and discussion

3.1. Characterisation of Mg-Al_2O_3 modified supports

The physico-chemical properties of the as-prepared MgO-modified alumina supports were investigated by WDXRF, XRD and N_2 physisorption.. The Mg loading as determined by WDXRF varied between 7 and 18%wt. (Table 1). The X-ray diffractograms of the supports are shown in Figure 1. As a reference the pattern of pure MgO is included as well. Expectedly all the samples displayed signals attributable to a cubic phase of gamma-alumina (2θ = 32.0, 37.7, 45.6 and 67.3º, JCPDS 01-074-2206). The samples with a Mg content of 12 and 18%wt. also showed distinct signals assignable to a cubic phase of magnesium oxide (JCPDS 00-004-0829) at 2θ = 43.0, 62.3, 74.7 and 78.6º. Note that the signal at 2θ = 37.0º could be ascribed to both Al_2O_3 and MgO phases. From the XRD peak intensity of the signals of MgO (2θ = 62.3º) and γ-alumina (2θ = 67.3º), which varied from 0.07 for the 7Mg/Al_2O_3 sample to 0.84 for the 18Mg/Al_2O_3 sample, it was verified that the relative amount of crystalline MgO increased with Mg loading. The MgO crystallite size was estimated from the full width half maximum of the characteristic peak located at 2θ = 42.9°, which corresponded to the (2 0 0) plane, by applying the Scherrer equation. Irrespective of the Mg content, the crystallite size was around 10-11 nm, which was half of that of pure magnesia (21 nm), thus evidencing a good dispersion of MgO over the surface of the alumina. On the other hand, the absence of segregated MgO in the pattern of the 7MgO-Al_2O_3 support was coherent with the proximity of its Mg loading to that theoretically required to form a MgO monolayer (about 10%wt.) [24]. On the other hand, the possible formation of $MgAl_2O_4$

due to the interaction between MgO and Al_2O_3 could be ruled out as the main signals of this spinel (2θ = 31.3, 36.9, 44.8, 59.4 and 65.2º, JCPDS 00-005-0672) were not observed. This was reasonably expected since the calcination temperature of the investigated Mg/Al_2O_3 samples was 600 ºC while the formation of the spinel is reported to occur above this temperature [25]. In this sense, the pattern of the 18Mg-Al_2O_3 calcined at 850 ºC (18Mg-Al_2O_3-850), on which the formation of $MgAl_2O_4$ was induced, is included in Figure 1 for the sake of comparison.

FIGURE 1

TABLE 1

The textural properties of the supports in terms of BET surface area, mean pore diameter and pore volume are listed in Table 1. In addition, the results corresponding to the pure MgO sample synthesised by precipitation are also included. The following values were obtained for the blank alumina support 136 $m^2\ g^{-1}$, 0.55 $cm^3\ g^{-1}$ and 123 Å. After MgO deposition, the surface area slightly increased up to 139-145 $m^2\ g^{-1}$, probably due to the contribution of its intrinsic porosity to the resultant support. In this sense, the pore size distributions of the supports (Figure S2, Supplementary material) evidenced the appearance of a fraction of small mesopores (with sizes around 30-40 Å) attributable to the high dispersion of magnesia, which in turn also exhibited a pore size distribution centred around that pore size range. A similar increase in surface area was found by Caloch et al. when studying MgO-Al_2O_3 supports prepared by homogeneous precipitation. This was assigned to the interaction of magnesium and aluminium oxides creating new narrow mesopores that contributed to the total surface area [28]. On the contrary, both pore volume and mean pore size were much more affected with a marked decrease from 0.55 to 0.44 $cm^3\ g^{-1}$ and 123 to 110 Å, respectively.

3.2. Characterisation of Co/Mg-Al_2O_3 catalysts

A set of Co/Mg-Al_2O_3 catalysts was prepared by precipitation with two Co loadings, namely 20 and 30%wt. For comparative purposes, four reference cobalt catalysts supported on bare alumina and magnesia (20Co/Al_2O_3, 20Co/MgO, 30Co/Al_2O_3 and 30Co/MgO) were also examined. Table 1 includes the composition of the synthesised catalysts as determined by WDXRF. It must be pointed out that the actual Mg loading of the Co/Mg-Al_2O_3 samples (3-11%wt.) was appreciably lower than that theoretically expected (5-14%wt.) due to a partial leaching of the promoter during the cobalt deposition step. This was verified by the significant presence of Mg in the filtrates after Co precipitation as evidenced by ICP-AES analysis.

Figures 2 and 3 show the diffractograms of the cobalt catalysts. These patterns were characterised by the presence of γ-alumina (2θ = 67.3º) and a spinel-like cobalt phase (Co_3O_4 and/or $CoAl_2O_4$), (2θ = 31.3, 37.0, 45.1, 59.4 and 65.3º, JCPDS 00-042-1467 and JCPDS 00-044-0160). Note that it was not possible to differentiate between these two oxides since both phase crystallise in the cubic structure. The MgO phase was only detected (2θ = 43.0 and 62.3º) over the catalysts with the highest content of magnesium, namely 20Co/18Mg-Al_2O_3 and 30Co/18Mg-Al_2O_3. Furthermore, a close-up view of the diffraction signals of the Co spinel phase in the patterns of the catalysts with a 20%wt.Co revealed a significant position shift with increasing Mg loading. This shift was noticed for all the signals attributed to this phase. For the sake of clarity only the signal located at around 2θ = 37.0º is shown in Figure 4. This signal was noted at 2θ = 37.1º for the catalyst supported on bare alumina (20Co/Al_2O_3) and progressively shifted towards 2θ = 36.9º, being this diffraction angle virtually coincident with that observed when cobalt was supported on pure magnesia (20Co/MgO). This finding suggested that the Co_3O_4 phase switched from a Co-alumina-type interaction (which resulted in the formation of

263 $CoAl_2O_4$) to a Co-magnesia-type interaction (which eventually involved a less favoured
264 formation of $CoAl_2O_4$) with increasing Mg loadings. This shift was also indicative of an
265 enlargement of the unit cell of the associated Co spinel phase, which was in agreement
266 with some extent of lattice distortion of the cobalt spinel phase (enlargement of the unit
267 cell size from 8.039 Å to 8.069 Å) due to the interaction with magnesia [26]. Moreover,
268 a progressive widening of these signals was observed, thereby suggesting some inhibition
269 of the crystallisation of the Co-phase [27].

270 FIGURE 2

271 FIGURE 3

272 FIGURE 4

273 The addition of increasing amounts of cobalt oxide led to an appreciable negative impact
274 on the textural properties of the resultant catalyst (Table 1). Hence, when compared with
275 the corresponding MgO-modified alumina support, the BET surface area decreased by
276 16-20% for the 20Co/Mg-Al_2O_3 catalysts and about 32% for the 30Co/Mg-Al_2O_3
277 catalysts. The same trend was observed for the mean pore size (29-38% for the 20Co/Mg-
278 Al_2O_3 catalysts and 36-46% for the 30Co/Mg-Al_2O_3 catalysts). These results clearly
279 indicated that the cobalt species deposited over the surface of the support gradually
280 blocked its largest pores with increasing metallic loading. On the other hand, when
281 compared with the reference bare alumina-supported cobalt catalysts (Table 1), no large
282 differences were noticed for the 20Co/Mg-Al_2O_3 samples (113-118 $m^2\ g^{-1}$ versus
283 120 $m^2\ g^{-1}$ over 20Co/Al_2O_3). For the catalysts with a larger Co content, a more noticeable
284 decrease impact was visible (91-99 $m^2\ g^{-1}$ versus 108 $m^2\ g^{-1}$ over 30Co/Al_2O_3).
285 The Raman spectra of the Co/Mg-Al_2O_3 catalysts are shown in Figure 5 (20Co/Mg-
286 Al_2O_3) and 6 (30Co/Mg-Al_2O_3). For the sake of comparison, the spectra of the Co/Al_2O_3
287 and Co/MgO counterpart catalysts and the bulk Co_3O_4 and $CoAl_2O_4$ samples are also

288 included. All the supported catalysts displayed the five Raman actives modes associated
289 with Co_3O_4, namely three F_{2g} modes located at 194, 519 and 617 cm^{-1}, and the E_g and A_{1g}
290 modes at 479 cm^{-1} and 687 cm^{-1}, respectively [28]. However, the Mg-containing catalysts
291 showed comparatively weaker and wider signals. In line with the XRD results, this feature
292 suggested a lattice distortion of the Co_3O_4 phase in these samples due to its interaction
293 with magnesium. On the other hand, a close-up view of the A_{1g} vibration mode (650-725
294 cm^{-1}) for the 20Co/Mg-Al_2O_3 catalysts clearly evidenced the presence of additional
295 shoulders attached to this peak at 705 and 725 cm^{-1} in the 20Co/Al_2O_3 sample (Figure 7).
296 These signals (denoted as A_{1g}*) were also visible for the bulk $CoAl_2O_4$ sample and are
297 usually attributed to some inversion degree in the structure of cobalt aluminate [29,30].
298 The absence of these signals for the Co/Mg-Al_2O_3 catalysts pointed out that these samples
299 contained lower amounts of $CoAl_2O_4$, owing to a lesser extent of the cobalt-alumina
300 interaction. In addition to that, the A_{1g} signal of the Mg-containing catalysts displayed an
301 initial bathochromic shift (7 cm^{-1}) with increasing magnesium loadings up to 5%wt.
302 (20Co/12Mg-Al_2O_3) that could be attributed to a change in the predominant cobalt-
303 support interaction, from cobalt-alumina to cobalt-magnesia [12]. For higher magnesium
304 loadings (11%wt.Mg, 20Co/18Mg-Al_2O_3), the signal returned to a very similar position
305 (683 cm^{-1}) to that of cobalt supported on pure magnesia (684 cm^{-1}), thus evidencing a
306 promotion of the interaction between cobalt and magnesium with increasing magnesium
307 concentration at the cost of the interaction between cobalt and aluminium.

308 FIGURE 5

309 FIGURE 6

310 FIGURE 7

311 The redox properties of the samples were investigated by means of H_2-TPR (Figures 8
312 and 9, Table 2). Note that the H_2 uptake corresponding to the pure supports (Al_2O_3 and

MgO) and MgO-modified alumina supports (Co/Mg-Al_2O_3) was negligible. For a better understanding of the influence of MgO deposition on the alumina support, the results corresponding to the catalysts supported on blank alumina and magnesia were firstly analysed. As for the samples supported on bare alumina (20Co/Al_2O_3 and 30Co/Al_2O_3), their TPR profiles evidenced two distinct H_2 uptakes. The consumption observed at 250-500 ºC was associated with the reduction of free Co_3O_4. In fact, two peaks could be ascertained in this temperature range at 300-325 and 400-425 ºC in agreement with the well-known two-step reduction of $Co_3O_4 \rightarrow CoO \rightarrow Co$ [31]. The uptake located at markedly higher temperatures (above 550 ºC) corresponded to the reduction of $CoAl_2O_4$, which was formed during the calcination step of the catalytic precursor [32]. The measured overall H_2 uptakes were 18.6 mmol H_2 g_{Co}^{-1} (20Co/Al_2O_3) and 20.0 mmol H_2 g_{Co}^{-1} (30Co/Al_2O_3), significantly lower than the theoretical value for the full reduction of cobalt species as Co_3O_4 exclusively (22.6 mmol H_2 g_{Co}^{-1}). At the same time, these values were larger than that corresponding to the exclusive presence of $CoAl_2O_4$ in the samples (17.0 mmol H_2 g_{Co}^{-1}). Judging from these findings, it was reasonable to believe that a mixture of both Co_3O_4/$CoAl_2O_4$ was formed on the samples that presented an overall degree of reduction of 82 and 88%, respectively.

FIGURE 8

FIGURE 9

TABLE 2

As for the Co/MgO samples, a distinct H_2 peak centred at 300 ºC was noticed irrespective of the cobalt content, which was related to the reduction of free Co_3O_4. A substantial H_2 consumption was also noticed in the 350-950 ºC temperature range. This broad band was assigned to the reduction of a non-stoichiometric Mg-containing spinel phase and/or a CoO-MgO solid solution [33]. Similarly to the behaviour of the catalysts supported on

bare alumina, it is worth pointing out the total H_2 consumption of the Co/MgO samples was also considerably lower (13.1 mmol H_2 g_{Co}^{-1} for 20Co/MgO and 14.5 mmol H_2 g_{Co}^{-1} for 30Co/MgO) than the theoretical uptake. This implied that a notable fraction of Co species in these samples was present in the form of highly stable, non-reducible solid solution with a reduction temperature above 950 ºC. Consequently, an overall degree of reduction of 58 and 64%, respectively, was estimated. Judging from these results, it could be said that cobalt-magnesia interactions were comparatively much stronger than those created between cobalt species and alumina.

The formation of CoO-MgO solid solution because of the diffusion of CoO into the MgO lattice was difficult to verify by XRD. No significant changes in the 2θ diffraction angles of the Co/MgO catalysts with respect to those of pure MgO were noted. Interestingly, an inspection of the 1000-1500 cm^{-1} region in the Raman spectra of these samples (20Co/MgO and 30Co/MgO) could reveal the presence of this solid solution. As shown in Figure 10, the spectrum of pure MgO displayed a band located at 1100 cm^{-1} that could be attributed to a two-phonon vibration induced by some disorder in the structure of magnesia [34,35]. When cobalt was deposited over the pure MgO, this disorder-induced band was still visible, along with additional bands centred at around 1250 and 1350 cm^{-1} that would imply an increase in the disorder of the structure of MgO due to insertion of cobalt ions and the subsequent formation of the solid solution [36].

FIGURE 10

Over the series of 20Co/Mg-Al_2O_3 catalysts, the total reducibility was enhanced with respect to the MgO-free sample (Table 2). In this way, a moderate increase by 5-10% was noticed. The largest promotion corresponded to the 20Co/12Mg-Al_2O_3 sample with an increase in the degree of reduction from 82% (20Co/Al_2O_3) to 91%. Furthermore, the onset of the reduction process of free Co_3O_4 significantly decreased by 35-50 ºC. This

363 shift was also more notable for the catalyst supported on 12Mg-Al_2O_3, as shown in Figure
364 11. Likewise a small shoulder at about 450-500 ºC was noticed over the 20Co/12Mg-
365 Al_2O_3 and 20Co/18Mg-Al_2O_3 samples. This evidenced that a minor fraction of deposited
366 cobalt species strongly interacted with the promoter. On the other hand, it was found that
367 the reduction band occurring at higher temperatures (above 550 ºC), which was an
368 evidence of the presence of $CoAl_2O_4$, was still noticed over the MgO-modified alumina
369 catalysts, although its relative intensity was somewhat lower with respect to the catalysts
370 supported over bare alumina.
371 The same redox characteristics and trends were also recognised over the series of catalysts
372 with 30%wt.Co (Figure 9). This set of samples displayed a slightly higher specific H_2
373 consumption (1-5%), which suggested that the overall reducibility was somewhat
374 favoured with higher cobalt loadings (Table 2). Similarly, the reduction process started at
375 lower temperatures with respect to the analogous catalyst supported on blank alumina
376 (20-35 ºC) (Figure 11). In general, the redox behaviour of free Co_3O_4 present in the
377 Co/Mg-Al_2O_3 catalysts tended to be more similar to that observed over the Co/MgO
378 instead of the Co/Al_2O_3 counterpart, thereby evidencing a change in the nature of the
379 cobalt-support interaction induced by the addition of magnesium to the alumina support
380 in agreement with the results from XRD and Raman spectroscopy.
381 FIGURE 11
382 An attempt was made to estimate the relative amount of each type of Co species present
383 in the various catalysts by deconvoluting the experimental TPR profiles. The threshold
384 temperature of 550 ºC was taken as criterion to distinguish between easily reducible
385 cobalt species (Region I) that would include free Co_3O_4 (200-450 ºC) and cobalt-MgO
386 species (450-550 ºC) and hardly reducible cobalt species (Region II) in the form of cobalt
387 aluminate (>550 ºC) [37]. The results are summarised in Table 2. It was interesting to

note that the amount of the first type of cobalt species increased when MgO was present on the support. This promotion was notable over the 20Co/Mg-Al_2O_3 (from 6.6 mmol H_2 g_{Co}^{-1} over 20Co/Al_2O_3 to 9.8 mmol H_2 g_{Co}^{-1} over 20Co/12Mg-Al_2O_3). On the contrary, it was less significant for the samples with 30%wt.Co (from 9.8 mmol H_2 g_{Co}^{-1} over 30Co/Al_2O_3 to 11-11.3 mmol H_2 g_{Co}^{-1} over 30Co/12Mg-Al_2O_3 and 30Co/18Mg-Al_2O_3). Simultaneously, increasing amounts of MgO led to a marked decrease in the fraction of hardly reducible $CoAl_2O_4$, which was about 8-12% lower for the Co/18Mg-Al_2O_3 samples. Hence, the coverage of alumina with MgO was shown to be efficient for partially inhibiting the strong interaction between Co_3O_4 and Al_2O_3 that could ultimately lead to the formation of cobalt aluminate.

3.3. Catalytic activity

The catalytic efficiency was characterised by monitoring the rise in conversion as a function of temperature under given reaction conditions (300 mL CH_4 g^{-1} h^{-1}, about 60000 h^{-1}). Figure 12 includes the corresponding conversion-temperature profiles of the investigated cobalt catalysts. The T_{50} value (temperature at which 50% conversion was attained) was used as an indicative of the relative reactivity of each sample (Table 3). It must be noticed that the oxidation of methane to exclusively CO_2 was always observed in the whole temperature range. The reaction started to appreciably occur above 400 ºC over the 20Co/Mg-Al_2O_3 catalysts and above 350 ºC over the 30Co/Mg-Al_2O_3 catalysts. Accordingly, at 600 ºC conversion values at around 65-80% and 80-95% were noted, respectively. The cobalt catalysts supported on modified alumina were more efficient than the corresponding alumina-supported counterparts regardless the Co content since the T_{50} values were lowered by 25-30 °C. Secondly, the samples with a 30%wt.Co were always more efficient irrespective of the support. For instance, T_{50} values were 525 and 550 °C

413 over the 30Co/12Mg-Al_2O_3 and the 20Co/12Mg-Al_2O_3 catalysts, respectively. It seems
414 reasonable to believe that the observed improvement in performance could be associated
415 with the substantially enhanced redox properties of the catalysts due to MgO coverage of
416 the alumina surface. Hence, the best results were found over the 30Co/12Mg-Al_2O_3
417 sample.

418 FIGURE 12

419 The specific reaction rate of the cobalt catalysts was calculated at 450 ºC (Table 3). This
420 temperature was selected since it resulted in conversion values lower than 20% for all the
421 samples. The estimated rates varied between 1.5-2.9 mmol h^{-1} g_{Co}^{-1} over the 20Co/Mg-
422 Al_2O_3 catalysts and between 2.7-3.5 mmol h^{-1} g_{Co}^{-1} over the 30Co/Mg-Al_2O_3 samples.
423 Note that the highest specific activity was found for the samples supported on
424 12Mg/Al_2O_3. As can be seen, the promotion of catalytic activity when adding MgO was
425 particularly marked in the former case since the reaction rate was doubled. Taking into
426 consideration that the oxidation of methane over cobalt oxide catalysts involves the
427 participation of highly active oxygen species [38], the observed increase in catalytic
428 activity was proposed to be connected to the amount of easily reducible cobalt species the
429 sample as expressed by the specific hydrogen uptake from Region I in the TPR profiles.
430 In this sense, Figure 13 shows that there was a reasonable good correlation between the
431 specific reaction rate with the H_2 consumption measured below 550 ºC, that corresponded
432 to active oxygen species involved in the reduction of free Co_3O_4 and unstable cobalt-MgO
433 species.

434 FIGURE 13

435 The apparent activation energy of the reaction over the investigated cobalt catalysts was
436 evaluated by applying the integral method. A first pseudo-order for methane and a zero
437 pseudo-order for oxygen were assumed on the basis of a simplified Mars–van Krevelen

438 kinetics for this reaction studied with a high O_2/CH_4 molar ratio [39,40]. The results are
439 listed in Table 3 while the corresponding plots for the linearized kinetic equation of the
440 integral reactor are shown in Figure 14. The activation energies for the magnesium-free
441 catalysts were relatively high, namely 104 and 90 kJ mol^{-1} over $20Co/Al_2O_3$ and
442 $30Co/Al_2O_3$ samples, respectively, due to their relatively high content of inactive cobalt
443 aluminate. However, with increasing magnesium loading for a given Co concentration, a
444 decline in the apparent activation energy was evident. The lowest values were found for
445 the $Co/12Mg\text{-}Al_2O_3$ catalysts (89 and 79 kJ mol^{-1} for $20Co/12Mg\text{-}Al_2O_3$ and $30Co/12Mg\text{-}$
446 Al_2O_3, respectively). Over the catalysts with the highest Mg loading and the catalysts
447 supported on pure MgO the apparent activation energy significantly increased up to 102-
448 112 kJ mol^{-1}. As illustrated in Figure 15, the observed trends of the dependence of the
449 activation energy with Mg loading of the sample pointed out that the catalytic behaviour
450 of Co_3O_4 crystallites in the two $Co/12Mg\text{-}Al_2O_3$ samples tended to show the highest
451 similarity to that exhibited by the oxide particles present in a bulk Co_3O_4 catalyst, which
452 gave an apparent activation energy of 74 kJ mol^{-1} [20,41]. This finding would be
453 consistent with the lowest abundance of inactive, hardly reducible cobalt species such as
454 $CoAl_2O_4$ and/or CoO-MgO solid solution on these two catalysts, and the concomitant
455 largest population of highly active cobalt species mainly in the form of Co_3O_4. In this
456 way, it could be established that the presence of $CoAl_2O_4$ would affect the performance
457 of Co/Al_2O_3 and $Co/7Mg\text{-}Al_2O_3$ catalysts while the formation of a stable CoO-MgO solid
458 solution would negatively impact the performance of $Co/18Mg\text{-}Al_2O_3$ and Co/MgO
459 samples.

460 FIGURE 14

461 TABLE 3

462 FIGURE 15

Finally, a stability test over a prolonged period of time (150 hours) was performed over the most active catalyst (30Co/12Mg-Al_2O_3) at 500 °C (Figure 16). After a small drop in conversion from 36 to 30% during the first 25 hours, the sample maintained a steady methane conversion for the remaining time on stream. This behaviour was consistent with an observed slight loss of surface area (about 10%, from 97 to 87 $m^2 g^{-1}$) that in turn was reflected in an alteration of the redox properties of the sample. Hence, although the overall H_2 uptake did not vary significantly, the reduction temperatures shifted somewhat higher temperatures (around 20 ºC). No enlargement of the crystallite size of the spinel phase was detected.

FIGURE 16

4. Conclusions

The effect of MgO addition on the catalytic behaviour of alumina supported catalysts for the combustion of trace amounts of methane has been examined. Magnesia was deposited onto the alumina support prior to Co_3O_4 incorporation. From the textural point of view no marked effect was noticed after incorporating varying amounts of MgO (7-18%wt.Mg), due to the intrinsic properties of this promoter. When cobalt was deposited over these modified supports magnesium oxide acted as a barrier limiting the interaction between cobalt and alumina, consequently reducing the formation of inactive cobalt aluminate. In addition to that, the cobalt-magnesium interaction was found to be more beneficial to the redox properties of free Co_3O_4 than the cobalt-alumina interaction. Hence, the onset temperature for reduction was lowered and the overall hydrogen uptake of the catalysts significantly increased. As a result, the catalysts supported on the modified supports exhibited a higher activity than those supported on bare alumina. The highest

reaction rate was achieved by the 30Co/Mg-Al_2O_3 catalyst, which was also deemed thermally stable for prolonged periods of operation.

Acknowledgements

The author wish to thank the financial support provided by the Ministry of Economy and Competitiveness (CTQ2016-80253-R), Basque Government (IT657-13) and the University of the Basque Country UPV/EHU, and the technical and human support provided by SGIker (UPV/EHU).

References

[1] P. Forster, V. Ramaswamy, in: S. Solomon, D. Qin, M. Manning, M. Marquis, K. Averyt, M.M.B. Tignor, H.L. Miller, Z.L. Chen (Eds.), Climate Change 2007: Working Group I: The Physical Science Basis, Cambridge Univ. Press, New York, 2007, pp. 234.

[2] X. Jiang, D. Mira, D.L. Cluff, Prog. Energy Combust. Sci. 66 (2018) 176-199.

[3] E. Long, X. Zhang, Y. Li, Z. Liu, Y. Wang, M. Gong, Y. Chen, J. Nat. Gas Chem. 19 (2010) 134-138.

[4] T. Korakianitis, A.M. Namasivayam, R.J. Crookes, Prog. Energ. Combust. 37 (2011) 89-112.

[5] R. Dumitru, F. Papa, I. Balint, D.C. Culita, C. Munteanu, N. Stanica, A. Ianculescu, L. Diamandescu, O. Carp, Appl. Catal. A Gen. 467 (2013) 178-186.

[6] X. Yang, Q. Gao, Z. Zhao, Y. Guo, Y. Guo, L. Wang, Y. Wang, W. Zhan, Appl. Catal. B Environ. 239 (2018) 373-382.

[7] S. Li, H. Liu, L. Yan, X. Wang, Catal. Commun. 8 (2007) 237-240.

[8] L.F. Liotta, H. Wu, G. Pantaleo, A.M. Venezia, Catal. Sci. Technol. 3 (2013) 3085-3102.

[9] L.F. Liotta, G. Di Carlo, G. Pantaleo, A.M. Venezia, G. Deganello, Appl. Catal. B Environ. 66 (2006) 217-227.

[10] F. Zasada, W. Piskorz, J. Janas, J. Grybos, P. Indyka, Z. Sojka, ACS Catal. 5 (2015) 6879-6892.

[11] Z. Pu, H. Zhou, Y. Zheng, W. Huang, X. Li, Appl. Surf. Sci. 410 (2017) 14-21.

[12] Z. Chen, S. Wang, W. Liu, X. Gao, D. Gao, M. Wang, S. Wang, Appl. Catal. A Gen. 525 (2016) 94-102.

[13] A.H.A.M. Videla, P. Stelmachowski, G. Ercolino, S. Specchia, J. Appl. Electrochem. 47 (2017) 295-304.

[14] M.A. Ulla, R. Spretz, E. Lombardo, W. Daniell, H. Knözinger, Appl. Catal. B Environ. 29 (2001) 217-229.

[15] T. Xiao, S. Ji, H. Wang, K.S. Coleman, M.L.H. Green, J. Mol. Catal. A Chem. 175 (2001) 111-123.

[16] Q. Wang, Y. Peng, J. Fu, G.Z. Kyzas, S.M.R. Billah, S. An, Appl. Catal. B Environ. 168-169 (2015) 42-50.

[17] B. Solsona, T.E. Davies, T. Garcia, I. Vázquez, A. Dejoz, S.H. Taylor, Appl. Catal. B Environ. 84 (2008) 176-184.

[18] J. Cheng, J. Yu, X. Wang, L. Li, J. Li, Z. Hao, Energ. Fuels 22 (2008) 2131-2137.

[19] H.G. El-Shobaky, M.A. Shouman, A.A. Attia, Colloids Surf. A Physicochem. Eng. Asp. 274 (2006) 62-70.

[20] M. Riad, Appl. Catal. A Gen. 327 (2007) 13-21.

[21] S. Ji, S. Ji, H. Wang, E. Flahaut, K.S. Coleman, M.L.H. Green, Catal. Lett. 75 (2001) 65-71.

[22] A. Choya, B. de Rivas, J.R. González-Velasco, J.I. Gutiérrez-Ortiz, R. López-Fonseca, Appl. Catal. B Environ. 237 (2018) 844-854.

[23] A. Choya, B. de Rivas, J.I. Gutiérrez-Ortiz, R. López-Fonseca, Catalysts 8 (2018) 427.

[24] D. Li, Y. Ding, X. Wei, Y. Xiao, L. Jiang, Appl. Catal. A Gen. 507 (2015) 130-138.

[25] D. Li, M. Lu, Y. Cai, Y. Cao, Y. Zhan, L. Jiang, Appl. Clay. Sci. 132-133 (2016) 243-250.

[26] D. Jiang, B. Zhao, Y. Xie, G. Pan, G. Ran, E. Min, Appl. Catal. A Gen. 219 (2001) 69-78.

[27] G. Ye, G. Oprea, T. Troczynski, J. Am. Ceram. Soc. 88 (2005) 3241-3244.

[28] B. Caloch, M.S. Rana, J. Ancheyta, Catal. Today 98 (2004) 91-98.

[29] G. Zou, Y. Xu, S. Wang, M. Chen, W. Shangguan, Catal. Sci. Technolog. 5 (2015) 1084-1092.

[30] Z. Fattah, M. Rezaei, A. Biabani-Ravandi, A. Irankhah, H.R. Arandiyan, Chem. Eng. Commun. 203 (2016) 200-209.

[31] Q. Liu, L. Wang, M. Chen, Y. Cao, H. He, K. Fan, J. Catal. 263 (2009) 104-113.

[32] X. Jiang, Y. Ma, Y. Chen, Y. Li, Q. Ma, Z. Zhang, C. Wang, Y. Yang, Spectrochim. Acta Part A Mol. Biomol. Spectrosc. 190 (2018) 61-67.

[33] V. D'Ippolito, G.B. Andreozzi, D. Bersani, P.P. Lottici, J. Raman Spectrosc. 46 (2015) 1255-1264.

[34] B. de Rivas, R. López-Fonseca, C. Jiménez-González, J.I. Gutiérrez-Ortiz, J. Catal. 281 (2011) 88-97.

[35] Y. Ji, Z. Zhao, A. Duan, G. Jiang, J. Liu, J. Phys. Chem. C 113 (2009) 7186-7199.

[36] Y. Zhang, H. Xiong, K. Liew, J. Li, J. Mol. Catal. A Chem. 237 (2005) 172-181.

[37] M. Wu, Y. Fu, W. Zhan, Y. Guo, Y. Guo, Y. Wang, G. Lu, Catalysts 7 (2017) 155.

[38] L. Wu, D. Jiao, J.-. Wang, L. Chen, F. Cao, Catal. Commun. 11 (2009) 302-305.

[39] E. Cazzanelli, A. Kuzmin, G. Mariotto, N. Mironova-Ulmane, J. Phys. Condens. Matter 15 (2003) 2045-2052.

[40] J.L. Ewbank, L. Kovarik, C.C. Kenvin, C. Sievers, Green Chem. 16 (2014) 885-896.

[41] F. Zasada, J. Janas, W. Piskorz, M. Gorczynska, Z. Sojka, ACS Catal. 7 (2017) 2853-2867.

[42] N. Bahlawane, Appl. Catal. B Environ. 67 (2006) 168-176.

571 [43] P. Stefanov, S. Todorova, A. Naydenov, B. Tzaneva, H. Kolev, G. Atanasova, D.
572 Stoyanova, Y. Karakirova, K. Aleksieva, Chem. Eng. J. 266 (2015) 329-338.
573 [44] J.R. Paredes, E. Díaz, F.V. Díez, S. Ordónez, Energ. Fuel. 23 (2009) 86-93.
574

CAPTIONS FOR TABLES AND FIGURES

Table 1. Composition and textural properties of the modified-alumina supports and the synthesised cobalt catalysts.

Table 2. H_2-TPR results of the synthesised cobalt catalysts.

Table 3. Kinetic results of the synthesised cobalt catalysts.

Figure 1. XRD profiles of the Mg-Al_2O_3 supports.

Figure 2. XRD profiles of the 20Co/Mg-Al_2O_3 catalysts.

Figure 3. XRD profiles of the 30Co/Mg-Al_2O_3 catalysts.

Figure 4. Close-up view of the 2θ = 35-39° region of the 20Co/Mg-Al_2O_3 catalysts.

Figure 5. Raman spectra of the 20Co/Mg-Al_2O_3 catalysts.

Figure 6. Raman spectra of the 30Co/Mg-Al_2O_3 catalysts.

Figure 7. Close up view of the Raman spectra in the 650-725 cm^{-1} region of the 20Co/Mg-Al_2O_3 catalysts.

Figure 8. H_2-TPR profiles of the 20Co/Mg-Al_2O_3 catalysts catalysts.

Figure 9. H_2-TPR profiles of the 30Co/Mg-Al_2O_3 catalysts catalysts.

Figure 10. Close-up view of the distortion-induced phonon region of the Raman spectra of pure MgO and 20Co/MgO and 30Co/MgO catalysts.

Figure 11. Relationship among the total H_2 uptake, reduction onset temperature and the Mg content of the synthesised cobalt catalysts.

Figure 12. Light-off curves of the synthesised cobalt catalysts.

Figure 13. Correlation between the specific reaction rate and the H_2 specific uptake at low temperature (<550 °C).

Figure 14. Pseudo-first order fit for the experimental data obtained over the synthesised cobalt catalysts.

Figure 15. Evolution of the apparent activation energy with the magnesium loading of the synthesised cobalt catalysts.

Figure 16. Stability test of the 30Co/12Mg-Al_2O_3 catalyst.

Sample	S_{BET}, $m^2\ g^{-1}$	V_{pore}, $cm^3\ g^{-1}$	D_{pore}, Å	Co, %wt.	Mg, %wt.
Al_2O_3	136	0.55	123	-	-
7Mg-Al_2O_3	145	0.50	115	-	6.7
12Mg-Al_2O_3	142	0.48	110	-	12.4
18Mg-Al_2O_3	139	0.44	110	-	17.8
MgO	80	0.19	106	-	60.3
20Co/Al_2O_3	120	0.34	94	21.7	-
20Co/7Mg-Al_2O_3	118	0.31	88	20.5	2.9
20Co/12Mg-Al_2O_3	113	0.34	95	21.0	5.4
20Co/18Mg-Al_2O_3	117	0.31	95	21.0	10.6
20Co/MgO	60	0.27	162	21.6	47.3
30Co/Al_2O_3	108	0.29	89	27.9	-
30Co/7Mg-Al_2O_3	99	0.27	87	28.7	3.0
30Co/12Mg-Al_2O_3	97	0.29	97	30.8	4.5
30Co/18Mg-Al_2O_3	91	0.28	102	28.3	7.8
30Co/MgO	47	0.16	204	31.9	41.1

604

605 TABLE 1

Catalyst	Total H_2 uptake, mmol g_{Co}^{-1}	Onset reduction temperature, ºC	Degree of reduction, %	Region I-H_2 uptake, mmol g_{Co}^{-1}	Region II-H_2 uptake, mmol g_{Co}^{-1}
20Co/Al_2O_3	18.6	275	82	6.6	12.0
20Co/7Mg-Al_2O_3	20.0	210	89	8.7	11.3
20Co/12Mg-Al_2O_3	20.6	205	91	9.8	10.8
20Co/18Mg-Al_2O_3	19.5	220	86	8.9	10.6
20Co/MgO	13.1	245	58	8.1	5.0
30Co/Al_2O_3	20.0	225	88	9.8	10.2
30Co/7Mg-Al_2O_3	20.7	195	92	10.3	10.4
30Co/12Mg-Al_2O_3	21.1	185	93	11.0	10.1
30Co/18Mg-Al_2O_3	20.7	205	92	11.3	9.4
30Co/MgO	14.5	240	64	9.9	7.6

606

607 TABLE 2

608

Catalyst	T_{50}, °C	Specific rate at 450 °C, mmol CH_4 g_{Co}^{-1} h^{-1}	E_a, kJ mol^{-1}
20Co/Al_2O_3	580	1.5	104
20Co/7Mg-Al_2O_3	560	2.5	92
20Co/12Mg-Al_2O_3	550	2.9	89
20Co/18Mg-Al_2O_3	550	2.4	102
20Co/MgO	550	2.2	112
30Co/Al_2O_3	550	2.7	90
30Co/7Mg-Al_2O_3	535	3.3	83
30Co/12Mg-Al_2O_3	525	3.5	79
30Co/18Mg-Al_2O_3	530	3.0	88
30Co/MgO	525	2.5	102

609

610 TABLE 3

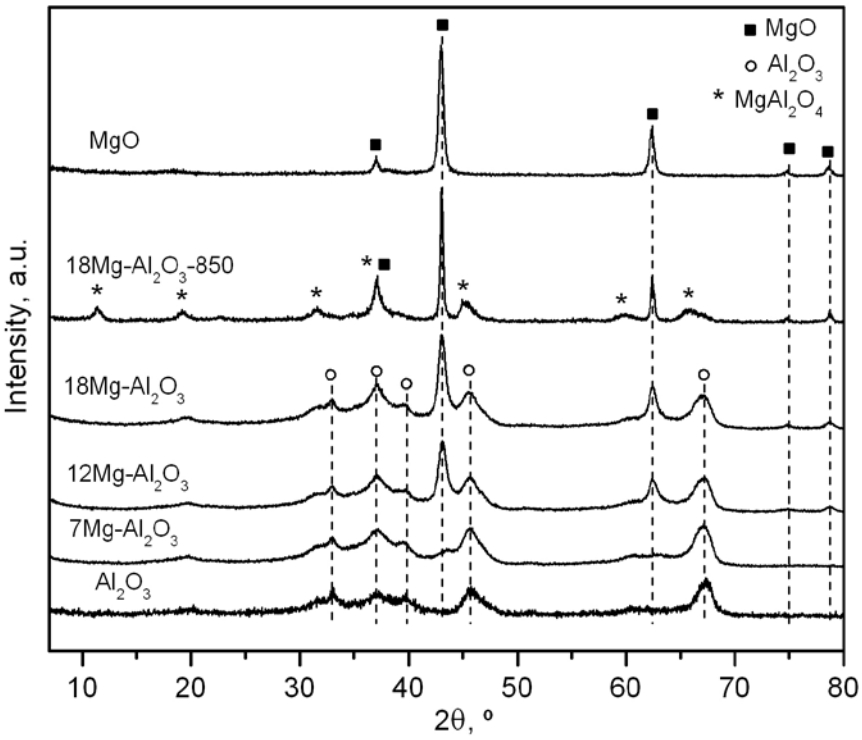

611

612 FIGURE 1

613

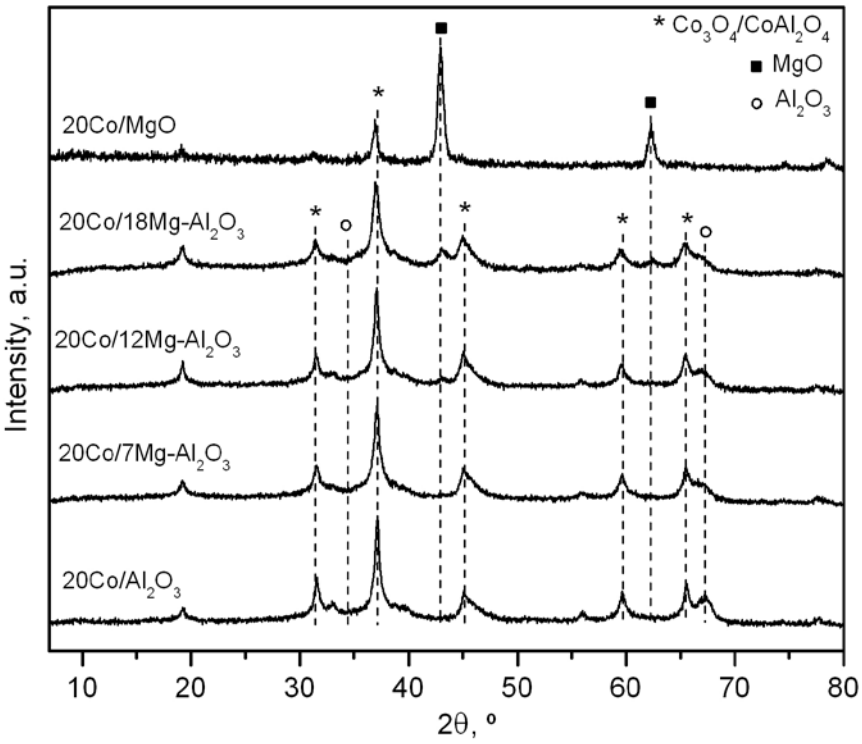

614

615 FIGURE 2

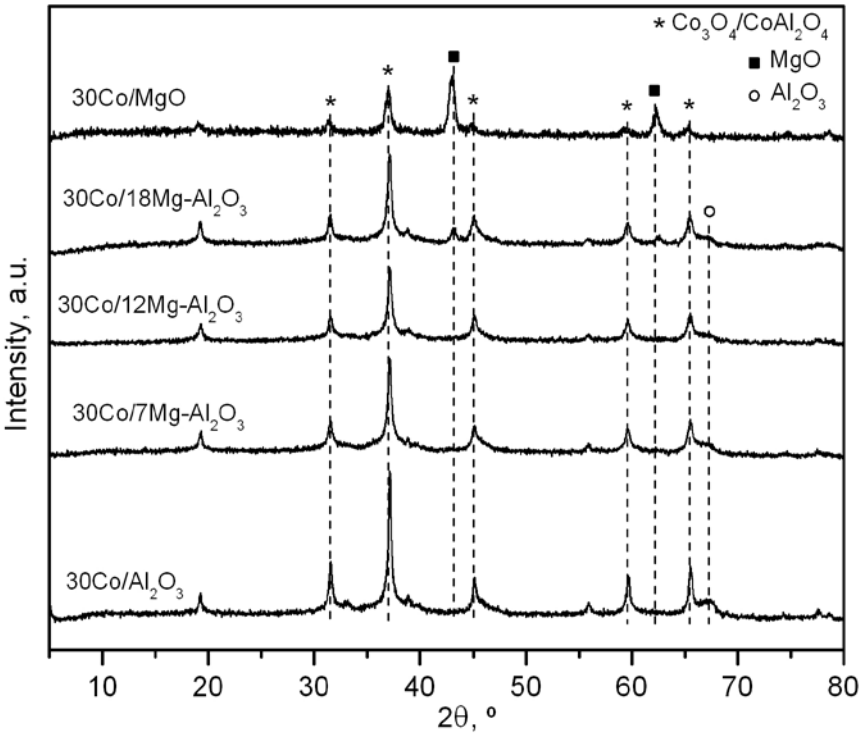

616

617 FIGURE 3

618

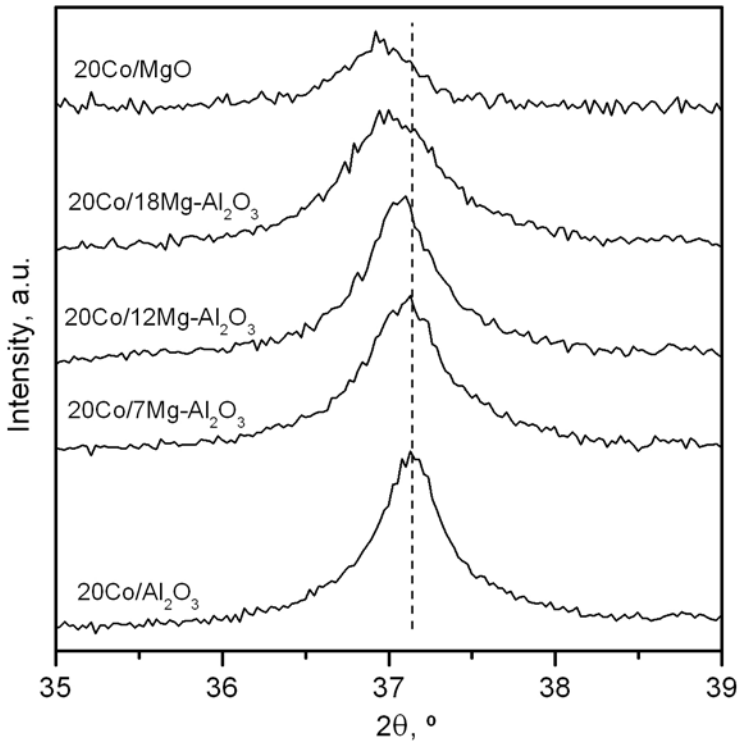

619

620 FIGURE 4

621

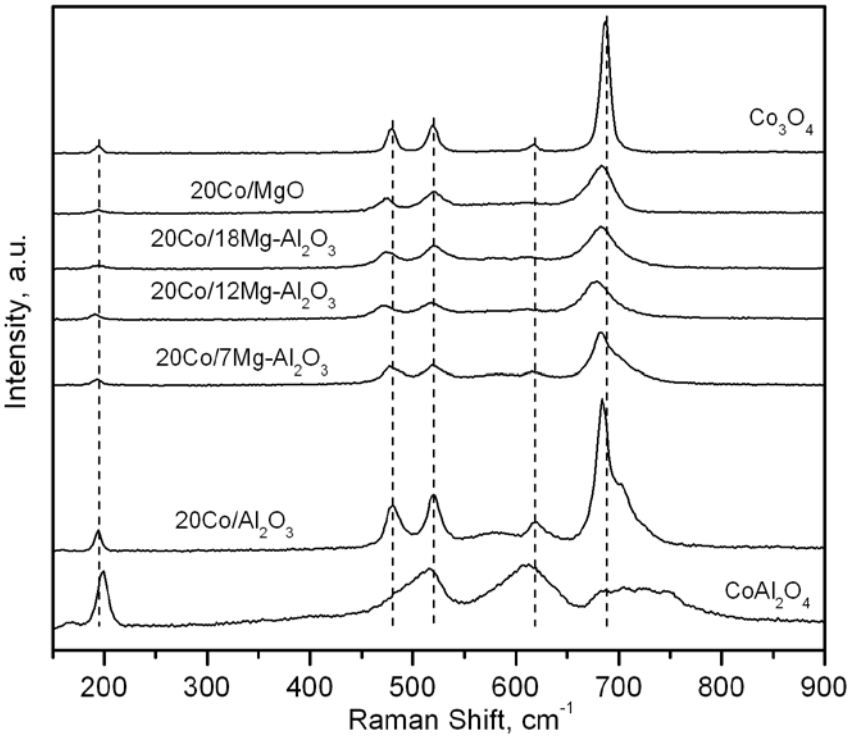

622

623 FIGURE 5

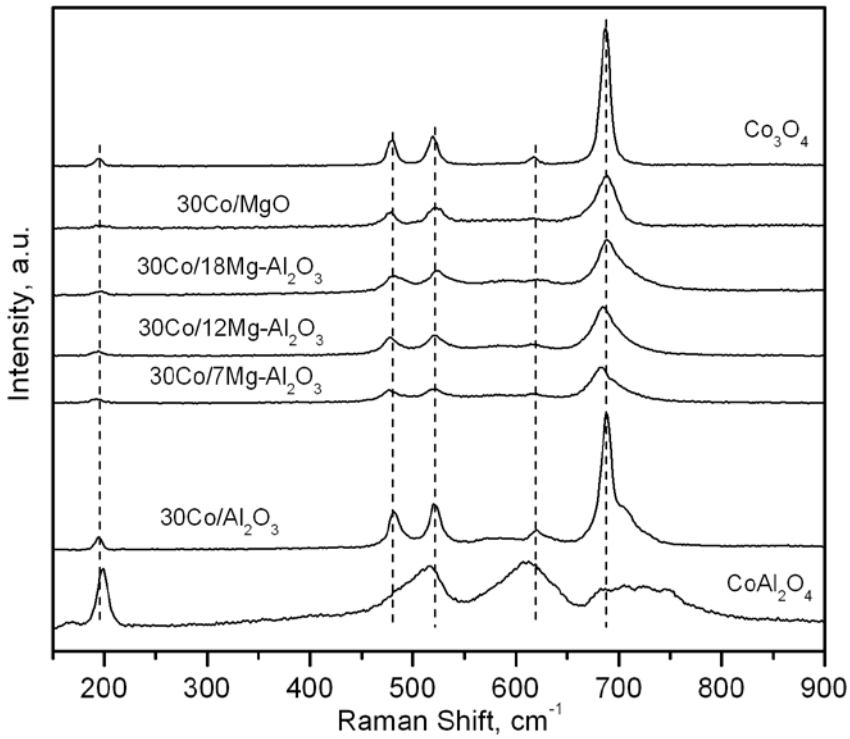

624

625 FIGURE 6

626

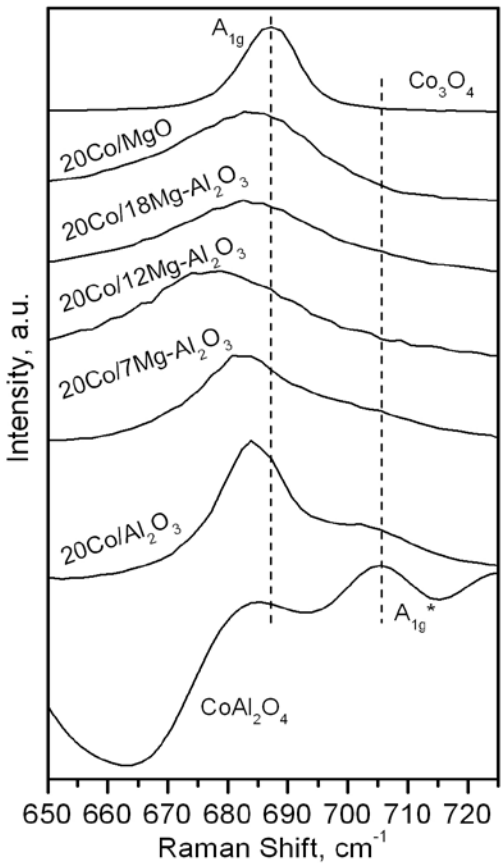

627

628 FIGURE 7

629

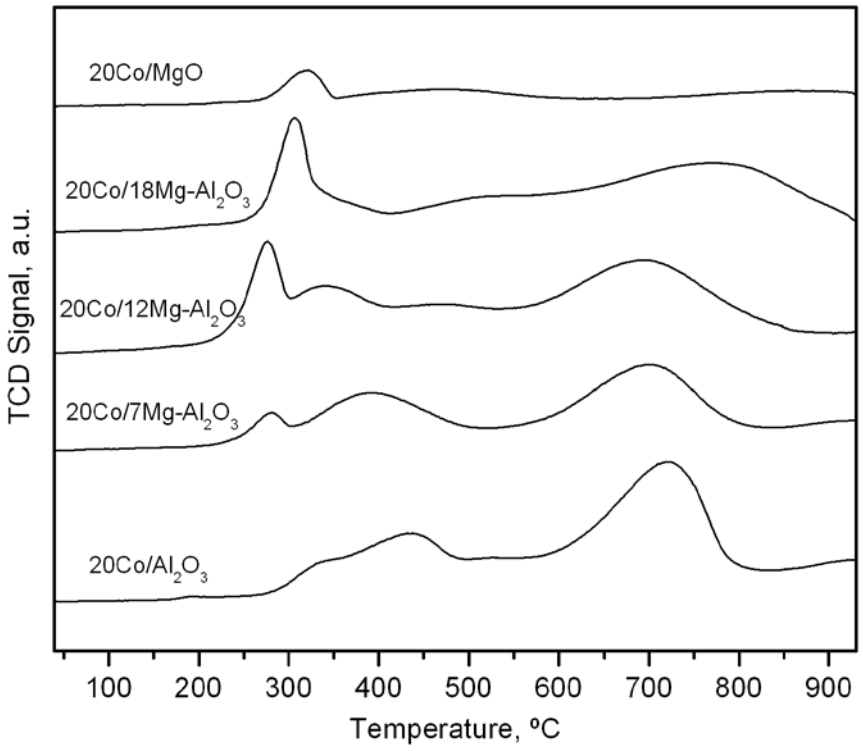

630

631 FIGURE 8

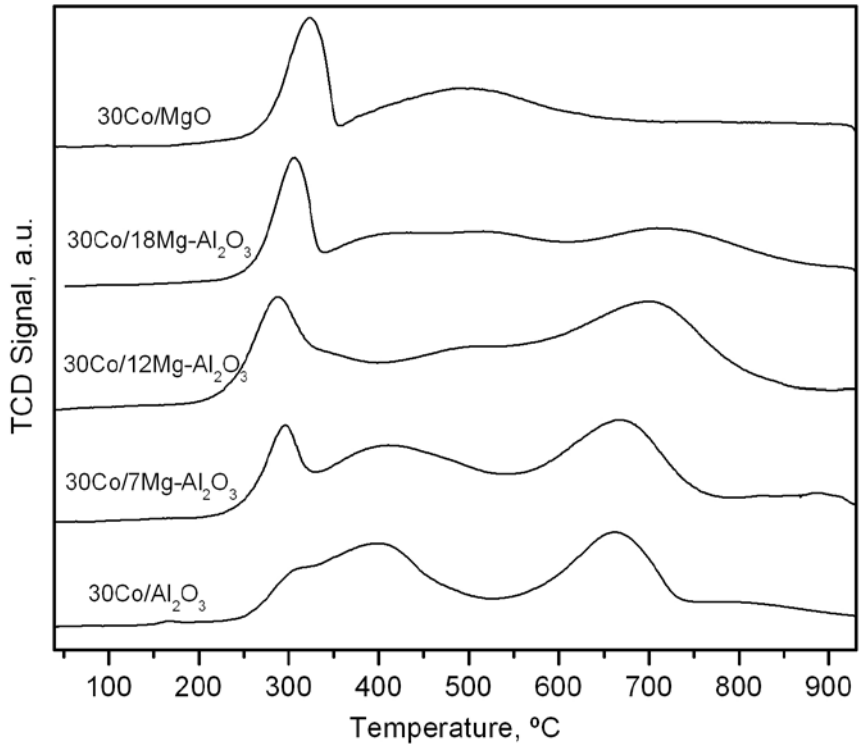

632

633 FIGURE 9

634

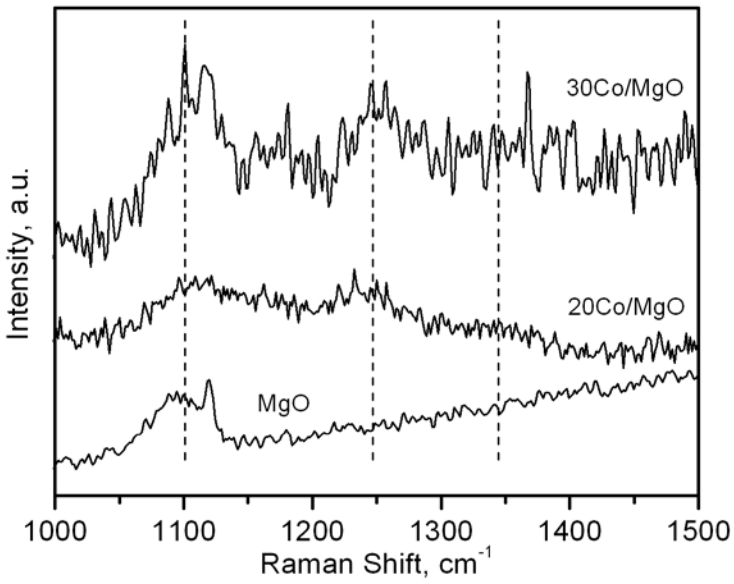

635

636 FIGURE 10

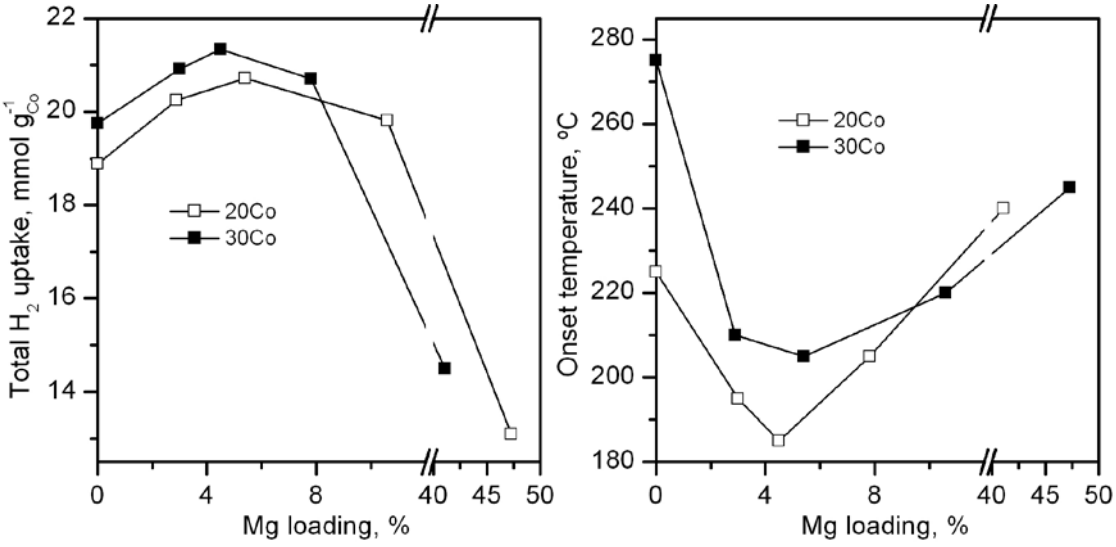

637

638 FIGURE 11

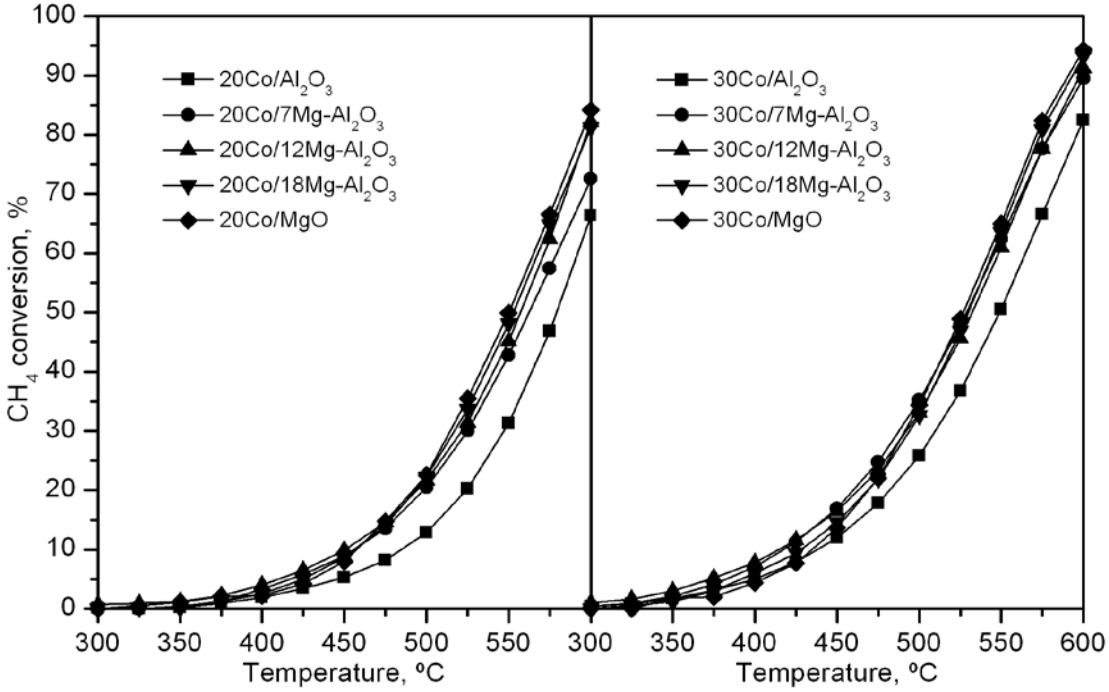

639

640 FIGURE 12

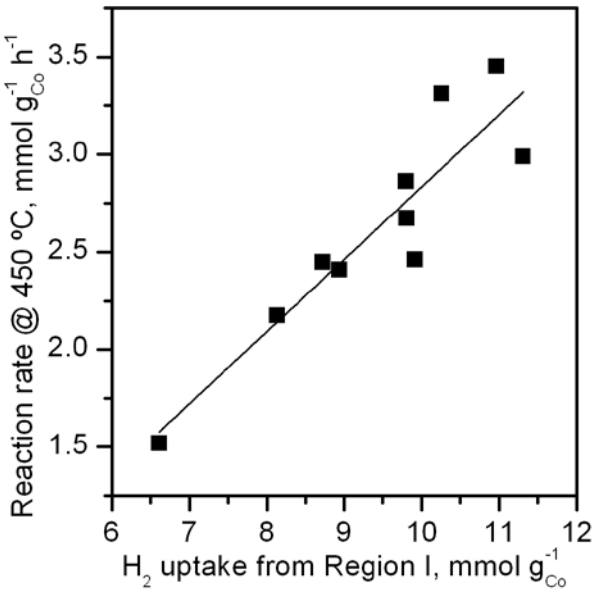

641

642 FIGURE 13

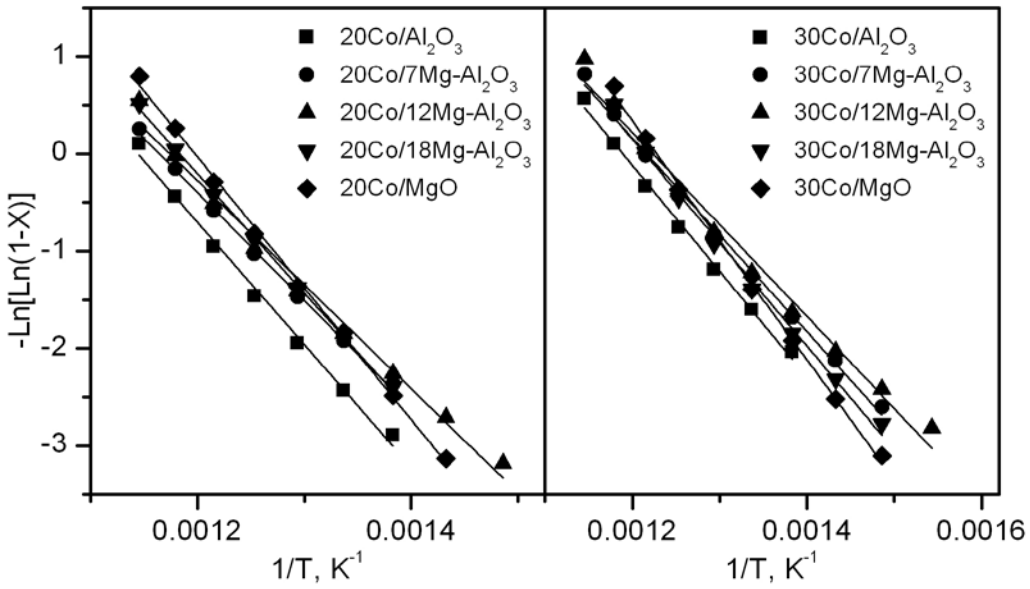

643

644 FIGURE 14

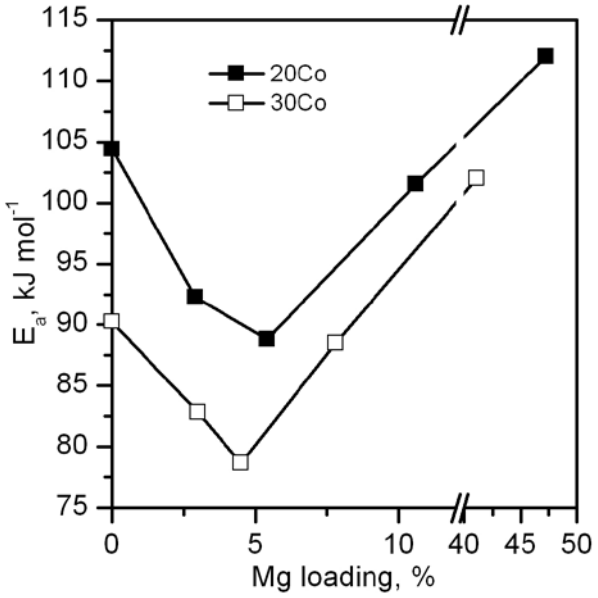

645

646 FIGURE 15

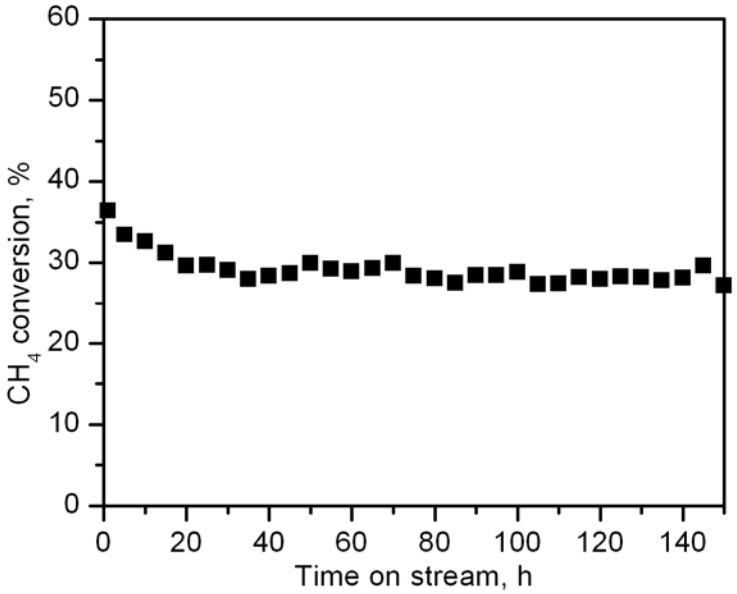

647

648 FIGURE 16